https://doi.org/10.5194/egusphere-2024-1330
Preprint. Discussion started: 17 May 2024

Quadratic Magnetic Gradients from 7-SC and 9-SC Constellations

Chao Shen[1], Gang Zeng[2], Rungployphan Kieokaew[3]

[1]School of Science, Harbin Institute of Technology, Shenzhen 518055, China
[2]School of Mathematics and Physics, Jingchu University of Technology, Jingmen, China
[3]Institut de Recherche en Astrophysique et Planétologie (IRAP), France

Correspondence to: Chao Shen (shenchao@hit.edu.cn), Gang Zeng (gzeng2014@126.com)

Abstract. To reveal the dynamics of magnetised plasma, it is essential to know the geometrical structure of the magnetic field, which is closely related to its linear and quadratic gradients. Estimation of the linear magnetic gradient requires at least four magnetic measurements, whereas calculation of the quadratic gradients of the magnetic field generally requires at least ten. This study is therefore aimed at yielding linear and quadratic gradients of the magnetic field based on magnetic measurements from nine-spacecraft HelioSwarm or seven-spacecraft Plasma Observatory constellations. Time-series magnetic measurements and transfer relationships between different reference frames were used to yield the apparent velocity of the magnetic structure as well as the components of the quadratic magnetic gradient along the direction of motion, while simultaneously elucidating the linear gradient and remaining components of the quadratic magnetic gradient using the least-squares method. Calculation via several iterations was applied to achieve satisfactory accuracy. The tests for the situations of magnetic flux ropes and dipole magnetic field have verifies the validity and accuracy of this approach. The results suggest that using time-series magnetic measurements from constellations comprising at least seven spacecraft and nonplanar configurations can yield linear and quadratic gradients of the magnetic field.

Key Points:

An iteration algorithm for the quadratic magnetic gradient based on measurement with constellations comprising at least seven spacecraft is presented.

Magnetic flux ropes and dipole magnetic field testing verifies the validity and accuracy of the approach.

Constellations containing at least seven spacecraft with nonplanar configurations are required for the approach.

Key Words: Multiple Spacecraft Measurements, Space Plasmas, Magnetic field, Quadratic Magnetic Gradient, Least Squares Method

https://doi.org/10.5194/egusphere-2024-1330
Preprint. Discussion started: 17 May 2024

1 Introduction

Multi-spacecraft constellations offer unique opportunities to observe plasma processes at various spatiotemporal scales simultaneously. Magnetic measurements *in situ* with multi-spacecraft constellations, in particular, allow the deduction of magnetic gradient such that fine magnetic structures, current densities, and magnetic geometries can be investigated. In general, magnetic measurements from constellations comprising at least four spacecraft forming a nonplanar configuration are required to deduce the three-dimensional linear gradient of a magnetic field (Harvey, 1998; Chanteur, 1998; Chanteur and Harvey, 1998; Shen et al., 2003; De Keyser, et al., 2007; De Keyser, 2008; Hamrin et al., 2008; Shen et al., 2012). Cluster (Escoubet et al., 1997, 2001) and Magnetospheric MultiScale (MMS; Burch et al., 2015) are four-spacecraft constellations that form tetrahedral configuration. Using the magnetic measurements of such the missions allows the linear gradient of the magnetic field, e.g., the current density distribution, to be estimated and the topology of the magnetic field to be further derived (Dunlop et al., 2002b; Shen et al., 2003, 2008, 2012, 2014; Shi et al., 2005; Runov et al., 2006; Shi et al., 2010; Zhang et al., 2011; Rong et al., 2011; Burch and Phan, 2016; Dong et al., 2018; Pitout and Bogdanova, 2021; Haaland et al., 2021). Furthermore, four-point magnetic field measurements can also be applied to determine the orientation and motion of planar discontinuities (Russell et al., 1983; Dunlop et al., 2002a; Sonnerup et al., 2004), as well as the geometry of curved boundary layers (Shen et al., 2020). For a planar constellation or a constellation comprising three spacecraft, only a two-dimensional linear magnetic gradient in the constellation plane can generally be derived (Vogt et al., 2009, 2013; Shen et al., 2012). Nevertheless, for certain structures such as one-dimensional and force-free structures, magnetic measurements from planar constellations or even Double Star constellations can also be reduced to a three-dimensional linear magnetic gradient (Vogt et al., 2009, 2013; Shen et al., 2012).

To obtain high-order gradients in the magnetic field, magnetic measurements from a constellation with more spacecraft are required. For the quadratic gradient of the magnetic field, which contains 18 components in total, a constellation with at least ten spacecraft is required to solve the system of equations (Chanteur, 1998; Shen et al., 2021b), with the limitation that not all spacecraft are simultaneously within the same quadratic surface (Zhou and Shen, 2024). Nevertheless, the quadratic gradient of a magnetic field can still be estimated from four-spacecraft constellations if additional current density measurements deduced from electron and ion measurements and certain physical constraints such as Ampère's law and Magnetic Gauss's law, are utilised (Liu et al., 2019; Torbert et al., 2020; Shen et al., 2021a). Utilising the linear and quadratic gradients of the magnetic field means that the complete geometry of a magnetic field can be determined (Shen et al., 2021a).

The HelioSwarm mission is a nine-spacecraft constellation consisting one hub (mothercraft) and eight nodes (daughtercraft) planned to be launched in 2029 by NASA. The swarm of nine spacecraft will allow for the first time simultaneous cross-scale observations of turbulent solar-wind plasmas in the vicinity of Earth. Specifically, each spacecraft of HelioSwarm will be

https://doi.org/10.5194/egusphere-2024-1330
Preprint. Discussion started: 17 May 2024

equipped with a Fluxgate magnetometer and a Search-Coil magnetometer, allowing comprehensive measurements of magnetic fields at 9 points simultaneously. Plasma Observatory is an ESA's new mission with a seven-spacecraft constellation in the Solar-Terrestrial environments, currently under Phase-A study. One important topic for these two new multi-spacecraft constellations is to ascertain how the linear and quadratic gradients of the magnetic field can be drawn from seven- or nine-point magnetic measurements, allowing the fine, nonlinear structures of the magnetic field in a space plasma to be identified. In this study, a new algorithm for calculating the linear and quadratic gradients of the magnetic field from seven- or nine-point magnetic measurements was derived using the least-squares method as well as an iterative approach that considers the reference frame transformation of the magnetic field.

The remainder of this paper is as follows. The new algorithm for calculating the linear and quadratic magnetic gradients from 7- or 9-point magnetic measurements is presented in Section 2; a description of the tests conducted for two typical magnetic structures: a cylindrical force-free flux rope and a dipole magnetic field, which were utilized to check the validity and accuracy of the new algorithm is given in Section 3; the error of the algorithm is evaluated in section 4; and finally, the conclusions are presented in Section 5.

2. Method

2.1 The scheme

Calculation of the linear and quadratic gradients of a magnetic field generally requires magnetic measurements from at least ten spacecraft; thus, using the magnetic measurements of nine-spacecraft (9S/C) HelioSwarm or seven-spacecraft (7S/C) Plasma Observatory constellation means that additional constraints are required. The transfer relationships between different references are the proper limitations used for completely determining the linear and quadratic gradients of magnetic field.

https://doi.org/10.5194/egusphere-2024-1330
Preprint. Discussion started: 17 May 2024

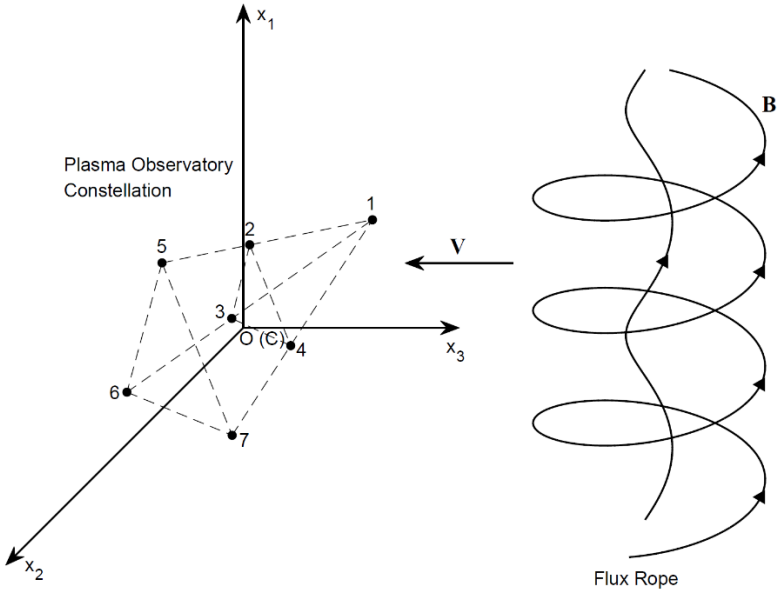

Figure 1. Schematic plot showing observation of a magnetic structure by the Plasma Observatory Constellation, which is composed of seven spacecraft. Barycentric coordinates are adopted; thus, the centre C of the constellation overlaps with the origin O of the Cartesian coordinates (x1,x2,x3) the magnetic structure is assumed to be moving at velocity V relative to the constellations, and the x3 axis is presumed to be anti-parallel to V.

The Taylor expansion of the magnetic field within two orders is expressed using:

$$\mathbf{B}(\mathrm{t},\mathbf{r}) = \mathbf{B}(\mathrm{t},\mathbf{r}_\mathrm{c}) + (\mathbf{r}\text{-}\mathbf{r}_\mathrm{c})\cdot\nabla\mathbf{B}(\mathrm{t},\mathbf{r}_\mathrm{c}) + \frac{1}{2}(\mathbf{r}\text{-}\mathbf{r}_\mathrm{c})\,(\mathbf{r}\text{-}\mathbf{r}_\mathrm{c})\cdot\nabla\nabla\mathbf{B}(\mathrm{t},\mathbf{r}_\mathrm{c}) \tag{1}$$

While the Taylor expansion of each component of the magnetic field is:

$$f_{(\alpha)} = f_c + x^i_{(\alpha)}(\nabla_i f)_c + \frac{1}{2}x^i_{(\alpha)}x^j_{(\alpha)}(\nabla_i\nabla_j f)_c = f_\mathrm{c} + x^i_{(\alpha)}g_i + \frac{1}{2}x^i_{(\alpha)}x^j_{(\alpha)}G_{ij} \tag{2}$$

Where f represents any one of the three components B^1, B^2, B^3 in the magnetic field **B**. The first order gradient is denoted $g_i \equiv (\nabla_i f)_c$ where (i=1, 2, 3) and the second order gradient $G_{ij} \equiv (\nabla_i\nabla_j f)_c$ where (i, j=1, 2, 3).

Conventionally, ten-point measurements are necessary to draw both the first- and second-order gradients of a physical quantity (Chanteur, 1998; Shen et al., 2021b); thus, additional physical constraints are required to obtain such measurements with the 9S/C HelioSwarm and 7S/C Plasma Observatory.

The following transformation relationship is used for the magnetic measurements:

$$\partial_t\mathbf{B} = -\mathbf{V}\cdot\nabla\mathbf{B}\,,\quad \partial_t\nabla\mathbf{B} = -\mathbf{V}\cdot\nabla\nabla\mathbf{B}\,, \tag{3}$$

https://doi.org/10.5194/egusphere-2024-1330
Preprint. Discussion started: 17 May 2024

This relationship allows both the apparent velocity **V** of the magnetic structure and the nine components of the quadratic magnetic gradient along the direction of motion, $\hat{\mathbf{V}}\cdot\nabla\nabla\mathbf{B}$ to be obtained (Shen et al., 2021a). The errors in formula (3) are on the order V/c.

2.1.1 The zeroth iteration

The temporal variation rate $\partial_t\mathbf{B}$ and first-order magnetic gradient $\left(\nabla\mathbf{B}\right)^{(0)}$ can readily be obtained from seven- or nine-point magnetic measurements, and the apparent velocity **V** of the magnetic structure and the longitudinal components of the second-order magnetic gradient, $\hat{\mathbf{V}}\cdot\nabla\nabla\mathbf{B}=\frac{1}{V}\partial_3\nabla\mathbf{B}$, can be deduced from the transformation relationship (3). Finally, the remaining nine components of the second-order magnetic gradient (i.e., the transverse components $G_{rs}^{(1)}=\left(\nabla_r\nabla_s f\right)^{(1)}$ where (r, s =1, 2)) can be determined from the seven- or nine-point magnetic measurements using the least squares method, allowing a first-order quadratic magnetic gradient $\left(\nabla\nabla\mathbf{B}\right)^{(1)}$ to be obtained.

2.1.2 The first order iteration

Provided with the zero-order quadratic magnetic gradient $\left(\nabla\nabla\mathbf{B}\right)^{(1)}$, the corrected first-order magnetic gradient $\left(\nabla\mathbf{B}\right)^{(1)}$ can be found using the least-squares method. Furthermore, the corrected apparent velocity $\mathbf{V}^{(1)}$ of the magnetic structure and the longitudinal components of the second-order magnetic gradient $\left(\hat{\mathbf{V}}\cdot\nabla\nabla\mathbf{B}\right)^{(2)}$ can be obtained from the transformation relationship (3). Again, the corrected transverse components of the quadratic magnetic gradient $\left(G_{rs}^{(2)}\left(r,s=1,2\right)\right)$ are obtained using the least-squares method, allowing a first-order quadratic magnetic gradient $\left(\nabla\nabla\mathbf{B}\right)^{(2)}$ to be obtained.

The iterations are performed repeatedly until satisfactory results are achieved.

For the 7S/C Plasma Observatory, the seven-point magnetic measurements yield 7 × 3=21 independent parameters, while the reference frame transformation provides nine constraints, resulting in 21+9=30 input parameters in total. The objective is to determine the magnetic field (three parameters), first-order gradient (nine parameters), and quadratic magnetic gradient (18 parameters) at the mesocentre of the constellation, a total of 3+9+18=30 parameters. Therefore, this scheme is reasonable. Clearly, the 9S/C magnetic measurements of HelioSwarm are sufficient to draw first-order and quadratic magnetic gradients using this method. These results indicate that the developed method is suitable for constellations comprising at least seven spacecraft.

https://doi.org/10.5194/egusphere-2024-1330
Preprint. Discussion started: 17 May 2024

2.2 Specific (operational) steps of the algorithm

Details of the steps used are given below.

2.2.1 The zeroth iteration:

Assume a linear approximation in space and let $G_{ij}^{(0)} = 0$. The magnetic field $\mathbf{B}_c^{(0)}$ and its linear gradient $(\nabla \mathbf{B})^{(0)}$ at the mesocentre of the constellation can then be obtained using the following formulas (Harvey, 1998; Shen et al., 2003):

$$B_{ci}^{(0)} = \frac{1}{N}\sum_{\alpha=1}^{N} B_{\alpha i}\ , \tag{4}$$

$$\left(\partial_i B_j\right)_c^{(0)} = \frac{1}{N}\sum_{\alpha=1}^{N} B_{\alpha i} r_{\alpha k} R_{kj}^{-1}\ . \tag{5}$$

where the volume tensor is $\mathrm{R_{kj}} = \frac{1}{\mathrm{N}}\sum_{\alpha=1}^{\mathrm{N}} \mathrm{r_{\alpha k}} \mathrm{r_{\alpha j}}$ or $\mathbf{R} \equiv \frac{1}{\mathrm{N}}\sum_{\alpha=1}^{\mathrm{N}} \mathbf{r}_\alpha \mathbf{r}_\alpha$, where N is the number of spacecraft within the constellation, and R_{kj}^{-1} s the inverse of the volume tensor R_{kj}. The determinant of the volume tensor is required to be nonzero, i.e., $\mathrm{R} = \det\left(R_{kj}\right) \neq 0$. This is equivalent to that the constellation is non-planar.

The temporal variation rate $\left(\partial_t \mathbf{B}\right)_c^{(0)}$ is readily obtained using time-series magnetic observation.

Now the frame transformation relationships (3) are reduced to the apparent velocity $\mathbf{V}^{(0)}$ of the magnetic structure and the longitudinal components of the quadratic magnetic gradient $\left(\partial_3 \nabla \mathbf{B}\right)^{(1)}$.

First, the zeroth approximation of the apparent velocity of the magnetic structure $\mathbf{V}^{(0)}$ can be found using the frame transformation relationship:

$$\left(\partial_t \mathbf{B}\right)^{(0)} = -\mathbf{V}^{(0)} \cdot \left(\nabla \mathbf{B}\right)^{(0)}, \tag{6}$$

Then, using the relationship:

$$\partial_t \left(\nabla \mathbf{B}\right)^{(0)} = -\mathbf{V}^{(0)} \cdot \left(\nabla \nabla \mathbf{B}\right)^{(1)}, \tag{7}$$

the longitude components of the quadratic magnetic gradient at first order can be drawn as:

https://doi.org/10.5194/egusphere-2024-1330
Preprint. Discussion started: 17 May 2024

$$\left(\partial_3 \nabla \mathbf{B}\right)_c^{(1)} = \frac{1}{V}\partial_t \left(\nabla \mathbf{B}\left(t, \mathbf{r}_c\right)\right)^{(0)}, \tag{8}$$

which are just $\left(G_{31}^{(1)}, G_{32}^{(1)}, G_{33}^{(1)}\right)$.

The remaining components of the quadratic magnetic gradients can be deduced using the least-squares method.

Assuming that:

$$S = \frac{1}{N}\sum_{\alpha=1}^{N}\left[f_c^{(0)} + x_{(\alpha)}^i g_i^{(0)} + \frac{1}{2} x_{(\alpha)}^i x_{(\alpha)}^j G_{ij}^{(1)} - f_{(\alpha)} \right]^2, \tag{9}$$

which can also be written as:

$$S = \frac{1}{N}\sum_{\alpha=1}^{N}\left[f_c^{(0)} + x_{(\alpha)}^i g_i^{(0)} - f_{(\alpha)} + \left(1 - \frac{1}{2}\delta_{i3}\right) x_{(\alpha)}^i x_{(\alpha)}^3 G_{i3}^{(1)} + \frac{1}{2} x_{(\alpha)}^p x_{(\alpha)}^q G_{pq}^{(1)} \right]^2. \tag{10}$$

If $\delta S = 0$, then

$$\frac{\partial S}{\partial G_{pq}} = \frac{1}{N}\sum_{\alpha=1}^{N} 2\left[f_c^{(0)} + x_{(\alpha)}^i g_i^{(0)} - f_{(\alpha)} + \left(1 - \frac{1}{2}\delta_{i3}\right) x_{(\alpha)}^i x_{(\alpha)}^3 G_{i3}^{(1)} + \frac{1}{2} x_{(\alpha)}^p x_{(\alpha)}^q G_{pq}^{(1)} \right] \cdot x_{(\alpha)}^p x_{(\alpha)}^q = 0. \tag{11}$$

which reduces to:

$$\begin{aligned} & f_c^{(0)} \sum_{\alpha=1}^{N} x_{(\alpha)}^p x_{(\alpha)}^q + \sum_{\alpha=1}^{N} x_{(\alpha)}^i x_{(\alpha)}^p x_{(\alpha)}^q g_i^{(0)} - \sum_{\alpha=1}^{N} f_{(\alpha)} x_{(\alpha)}^p x_{(\alpha)}^q + \sum_{\alpha=1}^{N}\left(1 - \frac{1}{2}\delta_{i3}\right) x_{(\alpha)}^i x_{(\alpha)}^3 x_{(\alpha)}^p x_{(\alpha)}^q G_{i3}^{(1)} \\ & + \frac{1}{2}\sum_{\alpha=1}^{N} x_{(\alpha)}^r x_{(\alpha)}^s x_{(\alpha)}^p x_{(\alpha)}^q G_{rs}^{(1)} = 0 \end{aligned} \tag{12}$$

Resulting in $G_{rs}^{(1)}\left(r, s = 1, 2\right)$, i.e., $\left(G_{21}^{(1)}, G_{22}^{(1)}, G_{11}^{(1)}\right)$.

The constellation must be nonplanar to achieve this result.

2.2.2 First order iteration

Assuming that:

$$S = \frac{1}{N}\sum_{\alpha=1}^{N}\left[f_c^{(1)} + x_{(\alpha)}^i g_i^{(1)} + \frac{1}{2} x_{(\alpha)}^i x_{(\alpha)}^j G_{ij}^{(1)} - f_{(\alpha)} \right]^2. \tag{13}$$

If $\delta S = 0$, then:

https://doi.org/10.5194/egusphere-2024-1330
Preprint. Discussion started: 17 May 2024

$$\frac{\partial S}{\partial f_c^{(1)}} = 0\,, \quad \frac{\partial S}{\partial g_i^{(1)}} = 0\,. \tag{14}$$

From $\frac{\partial S}{\partial f_c^{(1)}} = 0$, it can be assumed that:

$$\frac{1}{N}\sum_{\alpha=1}^{N}\left[f_c^{(1)} + x_{(\alpha)}^{i} g_i^{(1)} + \frac{1}{2} x_{(\alpha)}^{i} x_{(\alpha)}^{j} G_{ij}^{(1)} - f_{(\alpha)} \right] = 0\,. \tag{15}$$

Meaning that:

$$f_c^{(1)} = \frac{1}{N}\sum_{\alpha=1}^{N} f_{(\alpha)} - \frac{1}{2N}\sum_{\alpha=1}^{N} x_{(\alpha)}^{i} x_{(\alpha)}^{j} G_{ij}^{(1)} = \frac{1}{N}\sum_{\alpha=1}^{N} f_{(\alpha)} - \frac{1}{2} R^{ij} G_{ij}^{(1)}\,. \tag{16}$$

.

If $\frac{\partial S}{\partial g_i^{(1)}} = 0$, this can be reduced to:

$$\frac{1}{N}\sum_{\alpha=1}^{N}\left[f_c^{(1)} + x_{(\alpha)}^{i} g_i^{(1)} + \frac{1}{2} x_{(\alpha)}^{i} x_{(\alpha)}^{j} G_{ij}^{(0)} - f_{(\alpha)} \right] x_{(\alpha)}^{k} = 0\,, \tag{17}$$

i.e.,

$$\frac{1}{N}\sum_{\alpha=1}^{N} x_{(\alpha)}^{k} x_{(\alpha)}^{i} g_i^{(1)} + \frac{1}{2}\frac{1}{N}\sum_{\alpha=1}^{N} x_{(\alpha)}^{k} x_{(\alpha)}^{i} x_{(\alpha)}^{j} G_{ij}^{(0)} - \frac{1}{N}\sum_{\alpha=1}^{N} f_{(\alpha)} x_{(\alpha)}^{k} = 0\,. \tag{18}$$

The tensor $R^{kij} = \frac{1}{N}\sum_{\alpha=1}^{N} x_{(\alpha)}^{k} x_{(\alpha)}^{i} x_{(\alpha)}^{j}$ is then defined, resulting in:

$$R^{ki} g_i^{(1)} + \frac{1}{2} R^{kij} G_{ij}^{(0)} - \frac{1}{N}\sum_{\alpha=1}^{N} f_{(\alpha)} x_{(\alpha)}^{k} = 0\,. \tag{19}$$

Therefore, the first magnetic gradient is:

$$g_{\ell}^{(1)} = -\frac{1}{2}\left(R^{-1}\right)^{k\ell} R^{kij} G_{ij}^{(0)} + \left(R^{-1}\right)^{k\ell} \cdot \frac{1}{N}\sum_{\alpha=1}^{N} f_{(\alpha)} x_{(\alpha)}^{k}\,. \tag{20}$$

https://doi.org/10.5194/egusphere-2024-1330
Preprint. Discussion started: 17 May 2024

Using equation (3), it is now possible to obtain the corrected apparent velocity $\mathbf{V}^{(1)}$ of the magnetic structure and the longitudinal components of the corrected quadratic magnetic gradient $\left(\partial_3\nabla\mathbf{B}\right)^{(2)}$ $\left(\left(\partial_3\partial_i\mathbf{B}\right)^{(2)}\right)$, as in the zeroth iteration.

The least-squares method is then used to obtain the remaining nine components of the corrected quadratic magnetic gradient. If:

$$\begin{aligned} S &= \frac{1}{N}\sum_{\alpha=1}^{N}\left[f_{(c)}^{(1)} + x_{(\alpha)}^{i} g_i^{(1)} + \frac{1}{2} x_{(\alpha)}^{i} x_{(\alpha)}^{j} G_{ij}^{(2)} - f_{(\alpha)} \right]^2 \\ &= \frac{1}{N}\sum_{\alpha=1}^{N}\left[f_c^{(1)} + x_{(\alpha)}^{i} g_i^{(1)} - f_{(\alpha)} + \left(1 - \frac{1}{2}\delta_{i3}\right) x_{(\alpha)}^{i} x_{(\alpha)}^{3} G_{i3}^{(2)} + \frac{1}{2} x_{(\alpha)}^{p} x_{(\alpha)}^{q} G_{pq}^{(2)} \right]^2 \end{aligned} \tag{21}$$

Then $G_{pq}^{(2)}\left(p,q=1,2\right)$ can be obtained using the same procedure as that used for the zeroth iteration. So that all the components of the corrected quadratic magnetic gradient $\left(\nabla\nabla\mathbf{B}\right)^{(2)}$ are obtained.

Similarly, two or more iterations can be performed until stable linear and second-order magnetic gradients are obtained.

This algorithm requires that the constellation be composed of at least seven spacecraft and that its configuration is non-planar. Because both the 9S/C HelioSwarm and 7S/C Plasma Observatory satisfy these requirements, the linear and quadratic magnetic gradients can be readily obtained.

The Curlometer technique (Dunlop et al., 2002b) is used to calculate the current density based on multiple spacecraft magnetic measurements, with the relative error estimated by the ratio between the divergence and curl of the magnetic field, i.e., $\left|\frac{\nabla\cdot\mathbf{B}}{\nabla\times\mathbf{B}}\right|$. If the length and the magnetic field are normalized by the characteristic distance and magnetic strength $\left(D, B_0\right)$, the equation becomes $\left|\frac{\bar{\nabla}\cdot\bar{\mathbf{B}}}{\bar{\nabla}\times\bar{\mathbf{B}}}\right| \approx \left|\frac{\bar{\nabla}\cdot\bar{\mathbf{B}}}{1}\right| = \left|\bar{\nabla}\cdot\bar{\mathbf{B}}\right|$. Therefore, the dimensionless divergence of the magnetic field calculated with observation data can be regarded a reasonable measure of the relative error within the linear magnetic gradient. Similarly, the dimensionless $\left|\bar{\nabla}\left(\bar{\nabla}\cdot\bar{\mathbf{B}}\right)_c\right|$ can be used as a measure describing the relative error in the quadratic magnetic gradient derived using the method.

3. Comparison of new method with analytical modelling

In this section, the new method is applied to two analytical magnetic field models: a cylindrical force-free flux rope and a dipole magnetic field, to evaluate its validity and accuracy. The applicability of this approach was tested on the 7S/C Plasma

https://doi.org/10.5194/egusphere-2024-1330
Preprint. Discussion started: 17 May 2024

Observatory (N=7) under the assumption that the seven-spacecraft cluster crosses a magnetic field structure (as illustrated in Figure. 1) by comparing the linear and quadratic gradients of the magnetic field obtained by the new method with those obtained by accurate modelling.

The positions of the seven spacecrafts in the barycentric coordinate system were generated randomly with Cartesian coordinates between -0.02 and 0.02 R_E, as seen in Table 1. The 7S/C array is illustrated in Figure. 2.

Table 1. Coordinates of the seven spacecraft in the barycentre coordinate system, with α denoting spacecraft number.

α	$x_{(\alpha)}\,(R_E)$	$y_{(\alpha)}\,(R_E)$	$z_{(\alpha)}\,(R_E)$
1	0.0105	0.0016	0.0100
2	0.0135	0.0153	-0.0119
3	-0.0124	0.0155	-0.0026
4	0.0138	-0.0114	0.0139
5	0.0044	0.0157	0.0097
6	-0.0134	0.0152	0.0153
7	-0.0074	-0.0005	0.0052

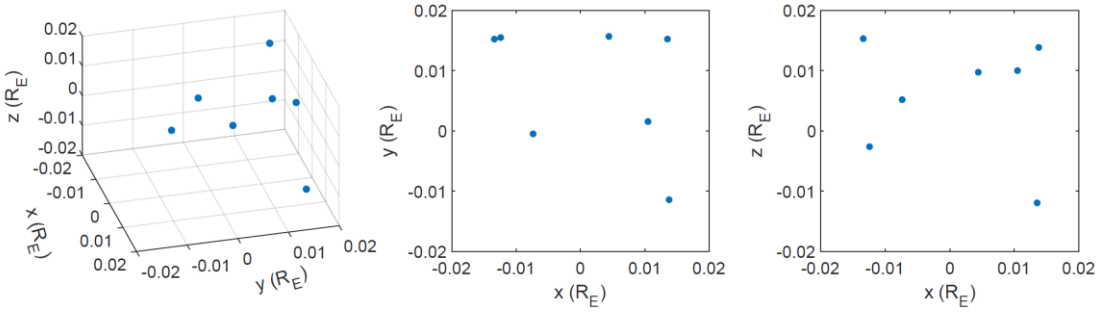

Figure 2. Configuration of the 7-S/C constellation.

The characteristic configuration of the spacecraft is described using several parameters. The three eigenvalues of the volumetric tensor R^{ij} are represented by w_1, w_2, and w_3 (where $w_1 \geq w_2 \geq w_3$) (Harvey, 1998), with their square roots representing the characteristic half-widths of the S/C in the three orthogonal directions along the corresponding eigenvectors (Harvey, 1998). The characteristic size of the S/C is twice the square root of the maximum eigenvalue, $L = 2\sqrt{w_1}$ (Robert et al., 1998; Shen et al, 2012). For the seven S/Cs in the cluster in this section, the three eigenvalues are $w_1 = 0.1643\,R_E^2$, $w_2 = 0.1104\,R_E^2$, and $w_3 = 0.0341\,R_E^2$, and the characteristic size is $L = 2\sqrt{w_1} = 0.0256\,R_E = 163.33\,\text{km}$.

https://doi.org/10.5194/egusphere-2024-1330
Preprint. Discussion started: 17 May 2024

3.1 Flux Rope

The flux rope was assumed to be force-free and cylindrically symmetrical. The magnetic field of the flux rope can be described using the Helmholtz equation, for which Lundquist (1950) provided analytical solutions in terms of the Bessel functions.

$$B_r = 0,\ B_\varphi(r) = B_0 J_1(\alpha r),\ B_z(r) = B_0 J_0(\alpha r)$$

where r is the radial distance from the centric axis; α is a constant, with $1/\alpha$ representing the characteristic scale of the flux rope; B_0 is the peak axial field intensity; and J_0 and J_1 are the zeroth- and first-order Bessel functions of the first kind, respectively. For this test, we set B_0=60 nT and $\alpha=1/R_E$.

The 7-S/C array was assumed to cross the flux rope in a straight line at uniform velocity. The array is represented by the barycentre with the red dot in Figure. 3, and moves from (-2, 0, 0) R_E to (2, 0, 0) R_E along the x-axis over a time interval of 100 s. The resolution of the magnetic field measurement was set to 1 s for the time-series observations, and the characteristic size of the 7-S/C array was set to L=0.0256 R_E for the gradients of the magnetic field at the barycentre along the trajectory to be obtained.

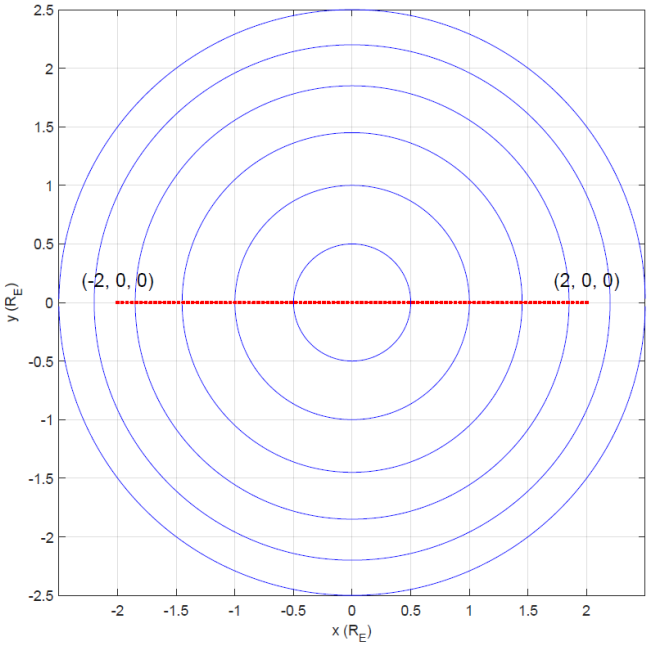

Figure 3. The cylindrical force-free flux rope crossing by the 7-S/C constellation as viewed from the axial direction. Trajectory of the barycentre of the constellation from (-2, 0, 0) R_E to (2, 0, 0) R_E over 100 s is shown by the red dotted line. Blue lines represent magnetic field lines.

The linear gradient of the magnetic field ($\nabla_i B_k$) has nine components, while the quadratic gradients ($\nabla_i \nabla_j B_k$) comprise 27 components. According to the analytical flux-rope model and symmetry of the quadratic gradients, only five independent

https://doi.org/10.5194/egusphere-2024-1330
Preprint. Discussion started: 17 May 2024

components of the quadratic gradients; $\nabla_1\nabla_2 B_1$, $\nabla_1\nabla_1 B_2$, $\nabla_2\nabla_2 B_2$, $\nabla_1\nabla_1 B_3$, and $\nabla_2\nabla_2 B_3$, and three components of the linear gradients $\nabla_2 B_1$, $\nabla_1 B_2$, and $\nabla_1 B_3$ are nonzero points on the *x*-axis when using Cartesian coordinates, simplifying the comparison between the gradients derived from the proposed method and the analytical model.

The impact of iteration on the results was investigated first, with the results at two different points used to demonstrate the variation in the relative errors under iteration, as illustrated in Figure. 4. The relative error is defined as $\left|\left(X_{algorithm} - X_{accurate}\right)\middle/ X_{accurate}\right| \times 100\%$, where $X_{algorithm}$ and $X_{accurate}$ represent the algorithm gradients derived using the new method and accurate values from the analytical model at the barycentre, respectively. As shown in Figure. 4(a) and 4(c), the linear gradients converged to certain values within 50 iterations, and the final relative errors were less than 0.02%. Figure 4(b) and 4(d) also indicate that the quadratic gradients converge. However, some quadratic gradients converged faster than others with fewer relative errors, and final relative errors of no more than 1.5% were obtained after 100 iterations. The maximum number of iterations was set to 100; thus, the gradients could be derived with good accuracy.

https://doi.org/10.5194/egusphere-2024-1330
Preprint. Discussion started: 17 May 2024

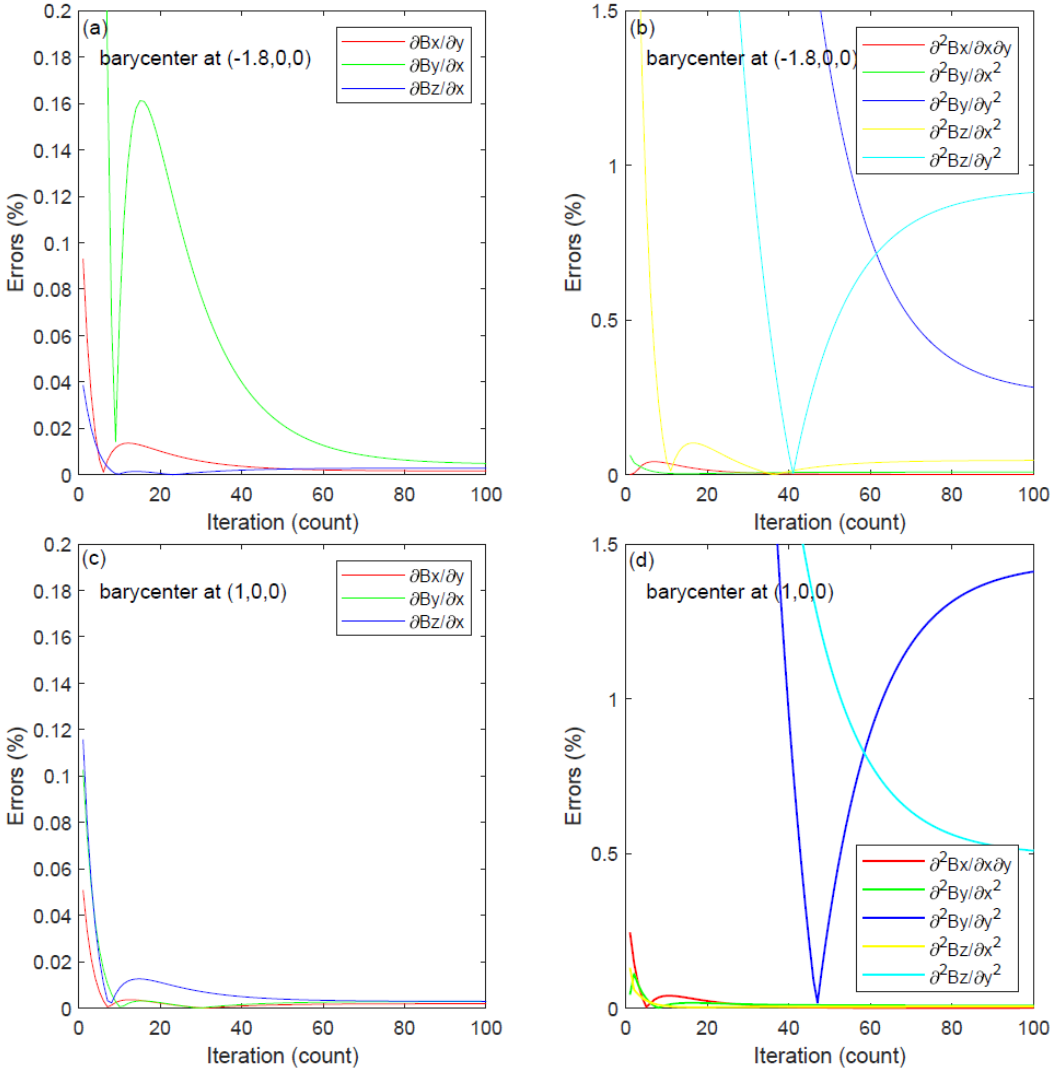

Figure 4. Relative errors in the nonzero components of the linear and quadratic gradients with different iteration numbers at different barycentre.

https://doi.org/10.5194/egusphere-2024-1330
Preprint. Discussion started: 17 May 2024

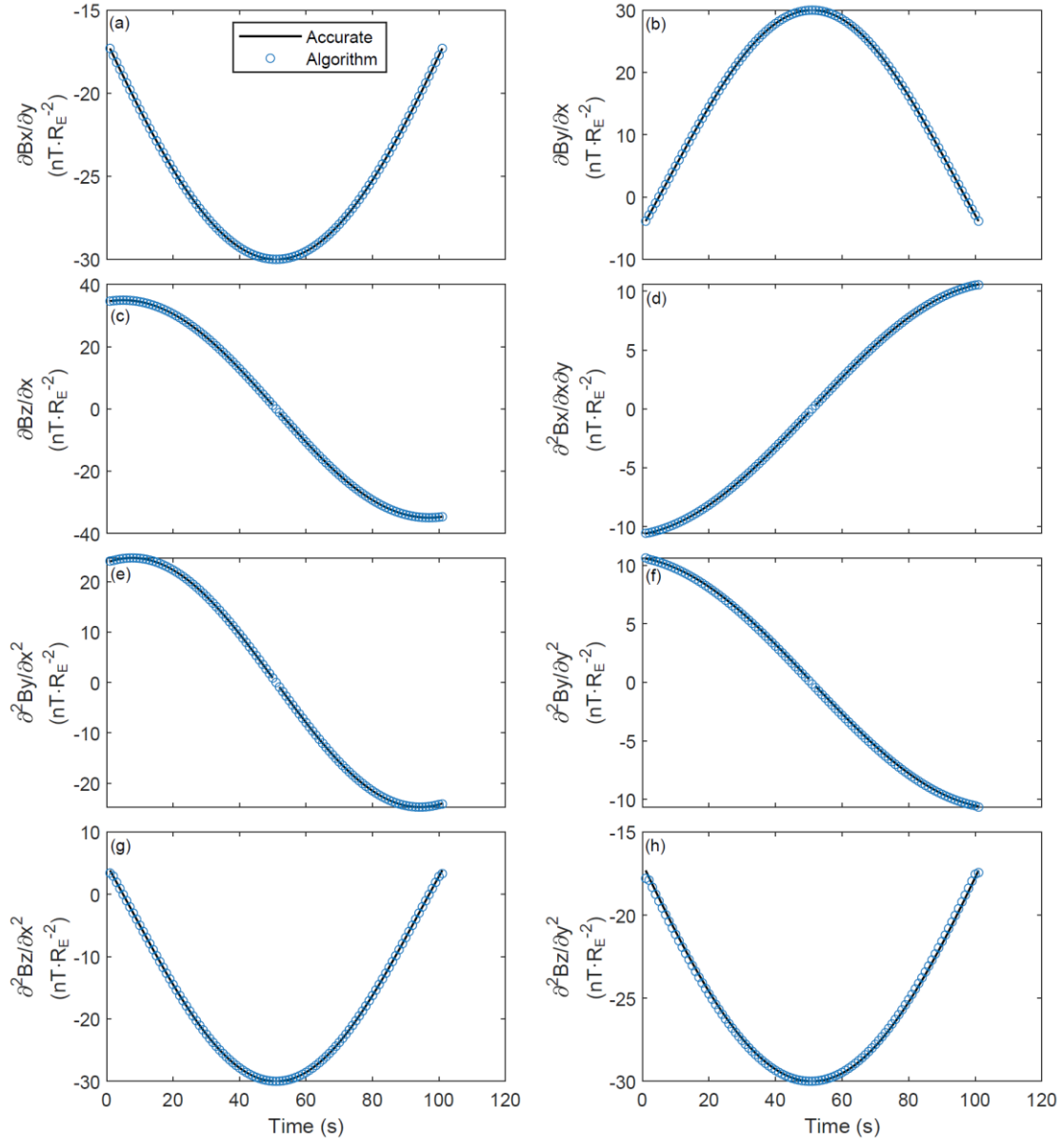

Figure 5. Time series showing nonzero components of the linear and quadratic gradients. Circles and solid lines represent the results obtained using the algorithm and accurate modelling, respectively.

Figure 5 shows a comparison of the nonzero linear and quadratic gradients at the barycentre derived from our method with those derived from the analytical model. The algorithm gradients are consistent with the accurate gradients, indicating that the proposed method is effective and precise when used with flux ropes.

https://doi.org/10.5194/egusphere-2024-1330
Preprint. Discussion started: 17 May 2024

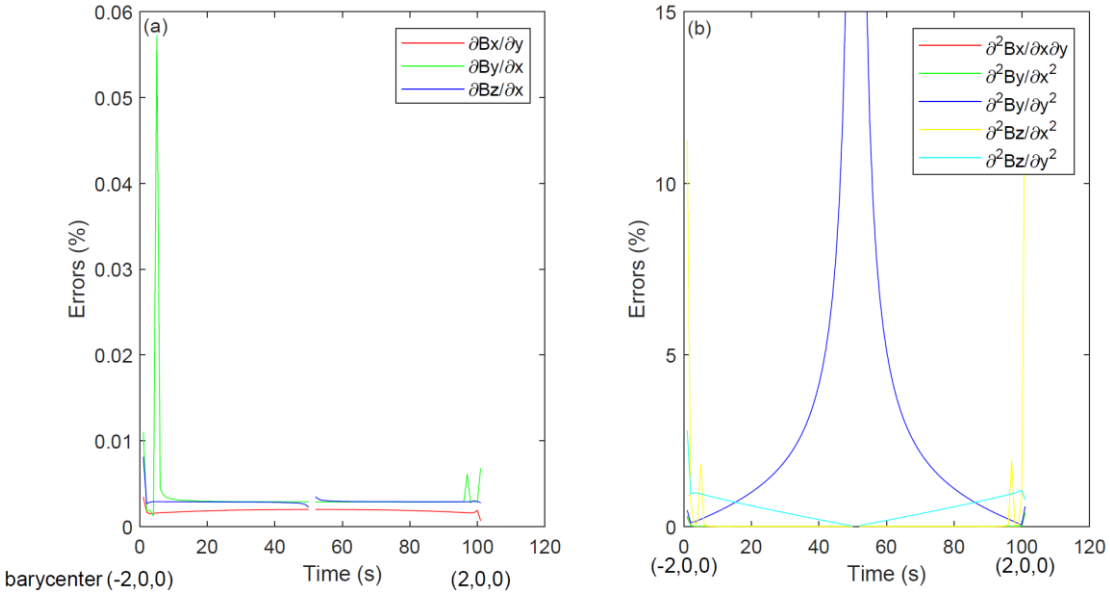

Figure 6. Relative errors in the nonzero components of the linear and quadratic gradients along the crossing path.

The relative errors of the gradients at points along the trajectory are shown in Figure. 6. All the relative errors of the linear gradients were less than 0.1%, and the vast majority of the relative errors for the quadratic gradients did not exceed 5%. It should be noted that the barycentre is at (0,0,0) at 50 s and that the nonzero components of the linear and quadratic gradients do not exist at (0,0,0). The barycentre is at (-0.04,0,0) R_E at 49 s, when accurate modelling and algorithm values for the quadratic gradient $\nabla_2\nabla_2 B_2$ of 0.3 and 0.1570 $\mathrm{nT}\cdot\mathrm{R}_E^2$, respectively. The relative error approaches 50%; however, the absolute error is low. Symmetrically, the situation described is the same as it would be if the barycentre were at (0.04,0,0).

3.2 Dipole field

The proposed method was also tested and verified using a magnetic dipole field. The geomagnetic dipole field is mathematically expressed as:

$$\begin{cases} B_x = -\dfrac{3xz}{r^5} B_0 \\ B_y = -\dfrac{3yz}{r^5} B_0 \\ B_z = \dfrac{r^2 - 3z^2}{r^5} B_0 \end{cases}$$

https://doi.org/10.5194/egusphere-2024-1330
Preprint. Discussion started: 17 May 2024

where B_0 is the magnetic field at the Earth's equator and is defined by $B_0 = \frac{\mu_0 M}{4\pi R_E^3} = 30008\ \text{nT}$; $M = 7.76\times10^{22}\ \text{A}\cdot\text{m}^2$ is the geomagnetic moment, with its direction set anti-parallel to the z-axis; x, y and z are the coordinates of the field points measured by R_E, and $r = \sqrt{x^2 + y^2 + z^2}$ is the radial distance from the origin measured by R_E.

The 7-S/C array was assumed to cross the dipole field in a straight line at constant velocity, with the barycentre parallel to the x-axis and moving from (-5, 0, 5) R_E to (5, 0, 5) R_E over 125 s, as illustrated in Figure. 7. The resolution of the magnetic field measurement was set to 1 s and the characteristic size of the 7-S/C array was set to 0.0256 R_E, which is the same as that of the flux-rope case, for the gradients of the magnetic field at the barycentre along the trajectory to be obtained.

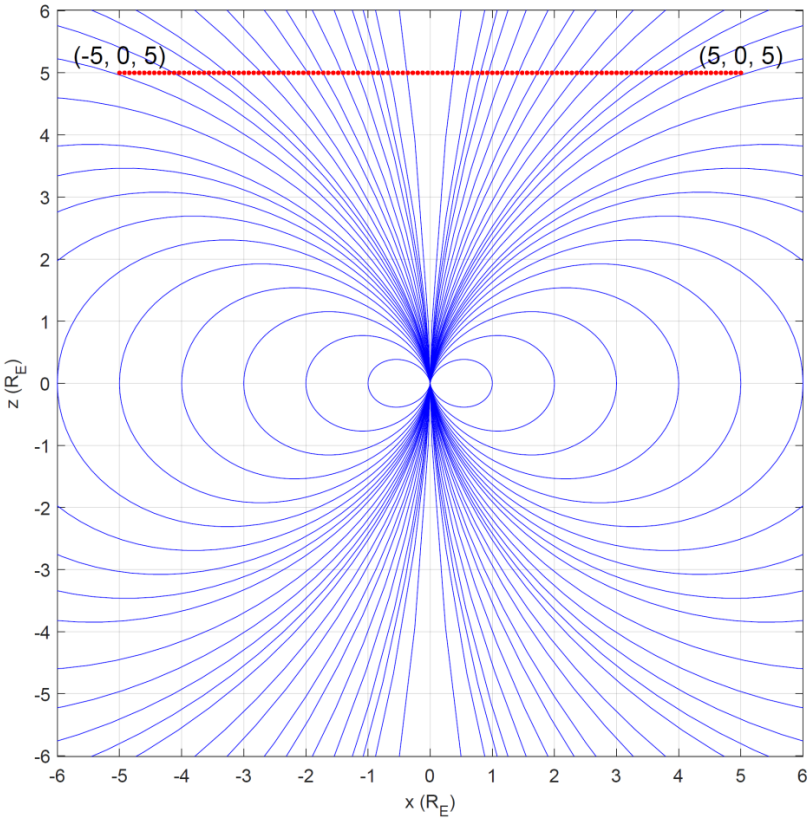

Figure 7. The magnetic dipole field crossed by the 7-S/C array. Trajectory of the barycentre of the 7-S/C array is from (-5, 0, 5) R_E to (5, 0, 5) R_E over 126 s as shown by the red dotted line. Blue lines represent magnetic field lines.

Only nonzero independent components are displayed, similar to the flux rope case. In view of the mathematical expression of the dipole field, ten independent components of the quadratic gradients and four independent components of the linear gradients were nonzero along the crossing path.

https://doi.org/10.5194/egusphere-2024-1330
Preprint. Discussion started: 17 May 2024

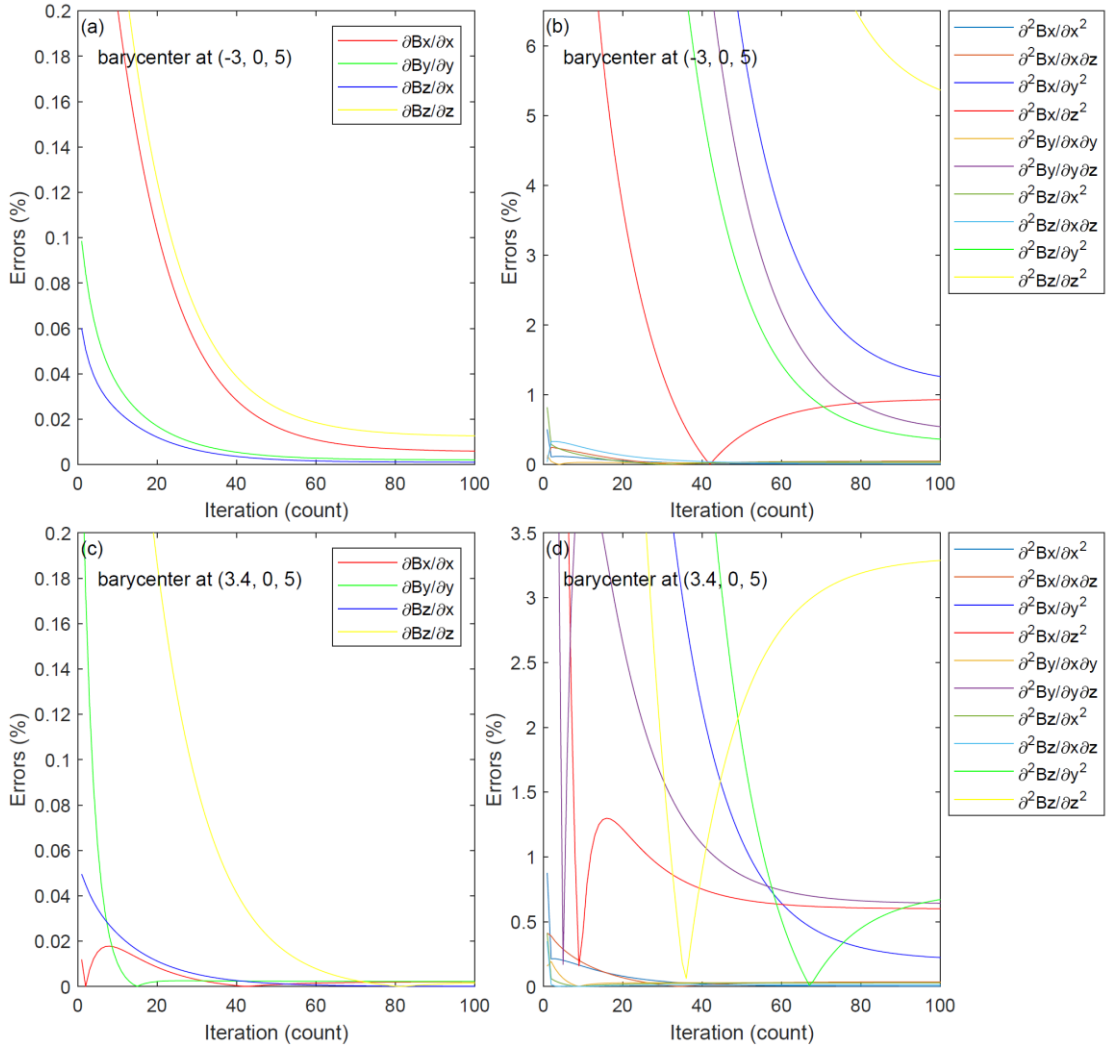

Figure 8. Relative errors in the nonzero components of linear and quadratic gradients with different iteration numbers at different barycentre.

Figure 8 shows the variation in the relative errors under iteration at two different points. As shown in Figure. 8(a) and 8(c), the linear gradients converged to certain values within 60 iterations, with final relative errors of less than 0.02%. Figure 8(b) and 8(d) show that the quadratic gradients also converge to low errors. After 100 iterations, most of the relative errors of the quadratic gradients were less than 1%, and the largest relative error was no more than 6%. These results suggest that it is reasonable to set the maximum number of iterations to 100 for the gradients to be derived with good accuracy in this case.

https://doi.org/10.5194/egusphere-2024-1330
Preprint. Discussion started: 17 May 2024

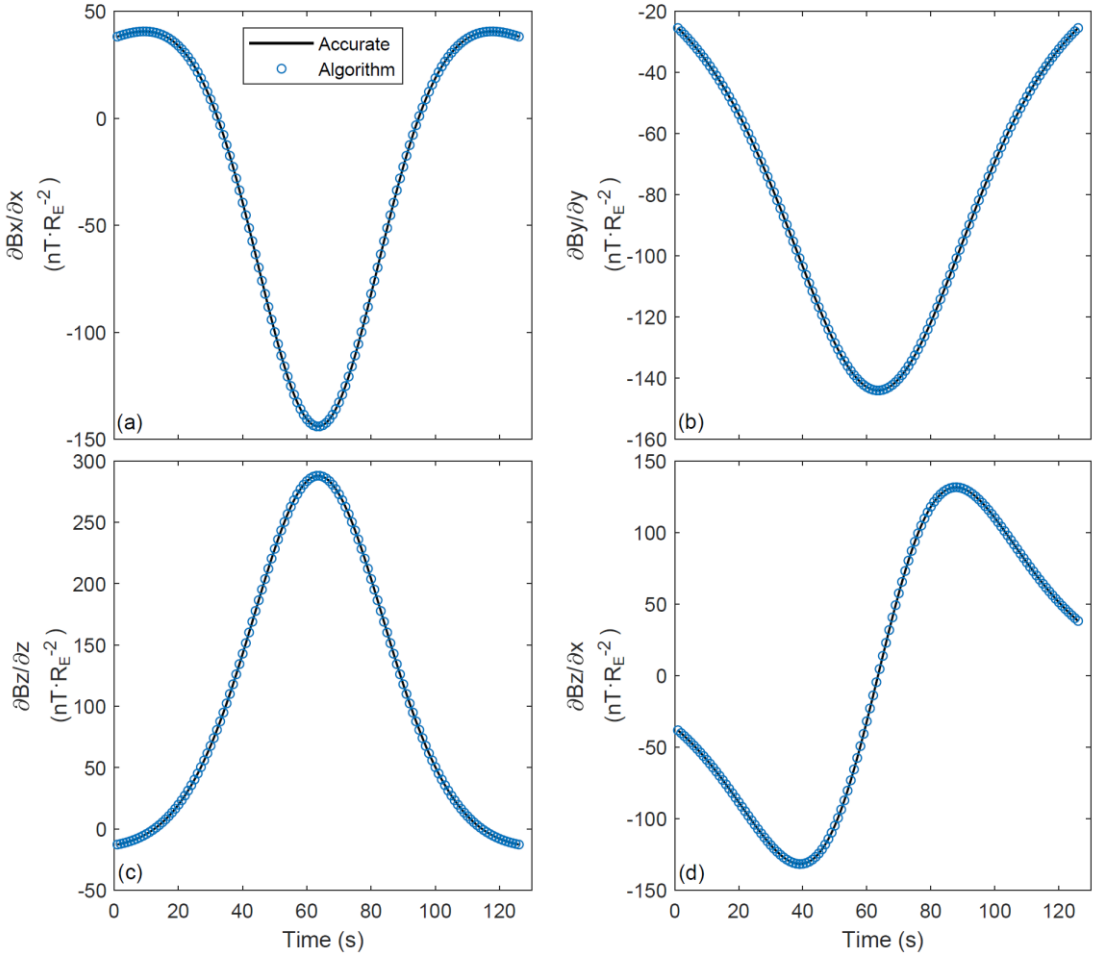

Figure 9. Time series showing nonzero components of the linear gradients. Circles and solid lines represent the results obtained using the algorithm and accurate modelling, respectively.

https://doi.org/10.5194/egusphere-2024-1330
Preprint. Discussion started: 17 May 2024

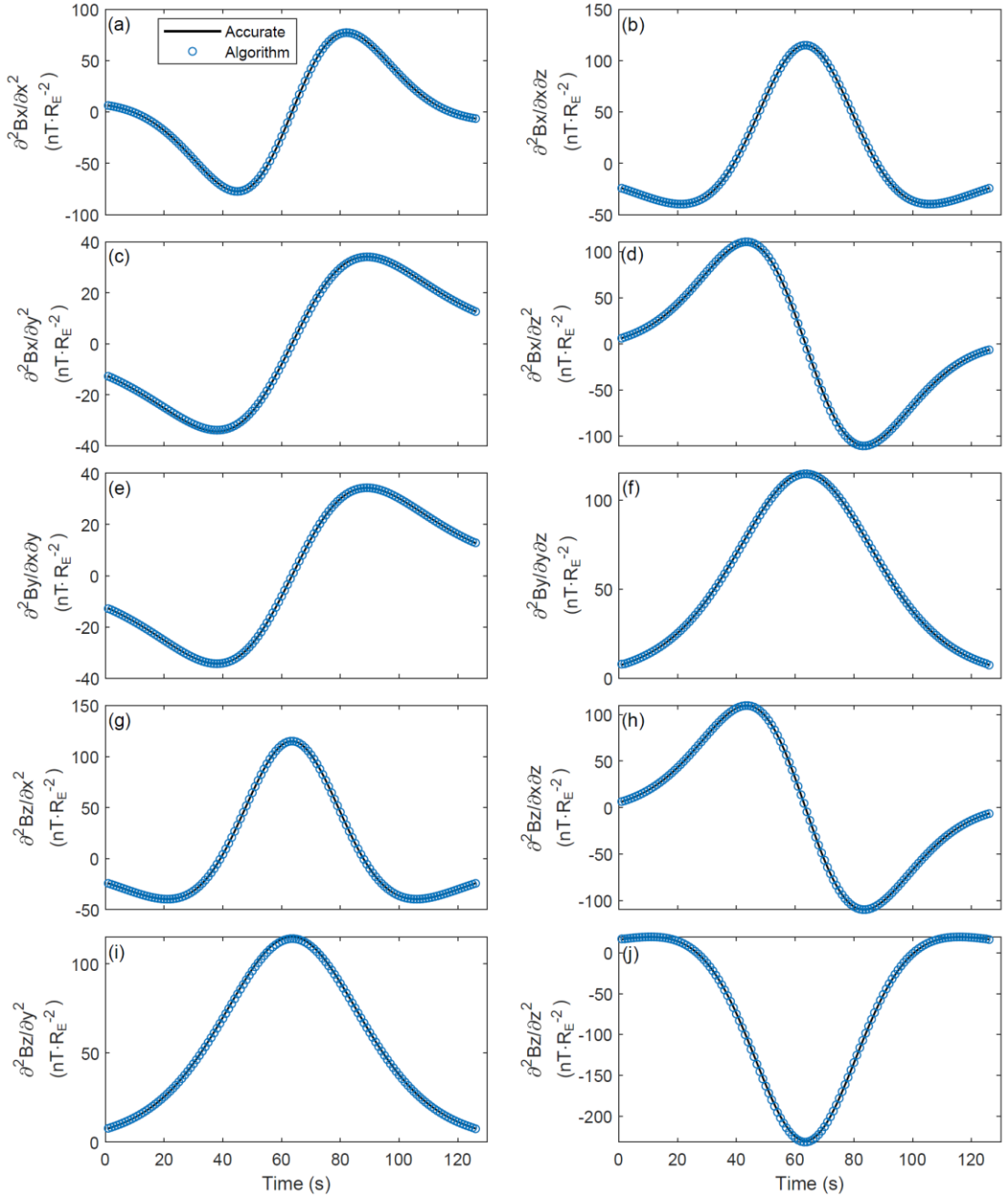

Figure 10. Time series showing nonzero components of the quadratic gradients. Circles and solid lines represent the results obtained using the algorithm and accurate modelling, respectively.

Figure 9 shows a comparison of the nonzero linear gradients derived from our method with those derived from the analytical model. A comparison of the nonzero quadratic gradients derived from the different sources is shown in Figure. 10. Both Figure.

https://doi.org/10.5194/egusphere-2024-1330
Preprint. Discussion started: 17 May 2024

9 and 10 indicate that the algorithm gradients are entirely consistent with those obtained from the accurate model, suggesting that the developed method is effective and precise for use with the dipole field.

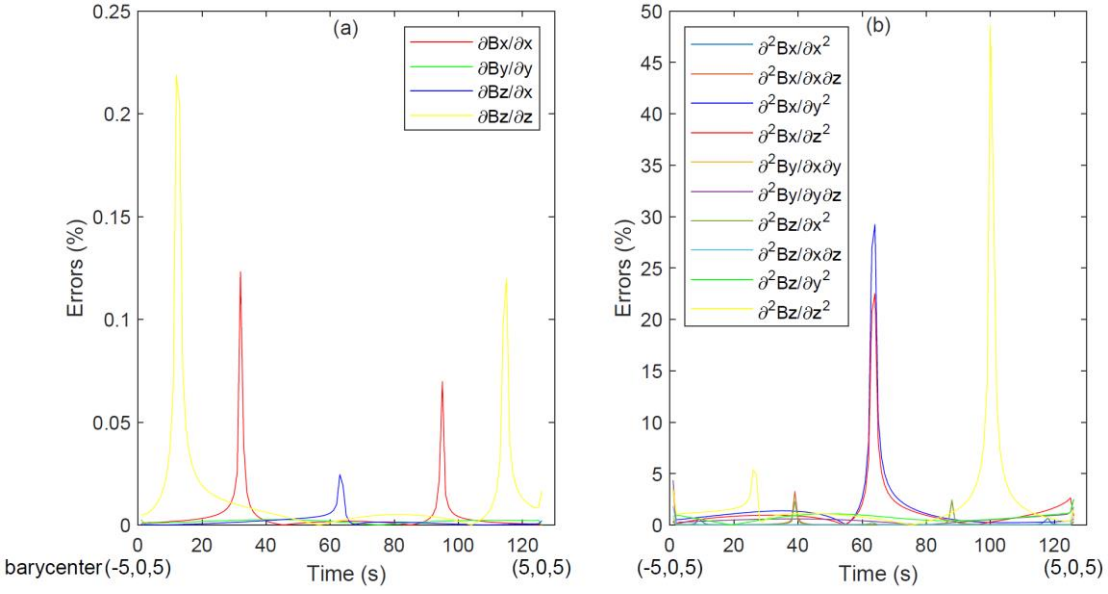

Figure 11. Relative errors in the nonzero components of the linear and quadratic gradients along the crossing path.

Figure 11 shows the relative errors of the gradients at the measured points along the crossing path. All the relative errors for the linear gradients were less than 0.25 %, and most of the relative errors in the quadratic gradients were less than 5%. It should be noted that the barycentre is at (2.92, 0, 5) R_E at 100s, and the accurate and algorithm quadratic gradients $\nabla_3\nabla_3 B_3$ are -1.2584 and -0.6461 $\mathrm{nT}\cdot\mathrm{R}_E^2$, respectively. The relative error approaches 50%; however, the absolute error is low. The barycentre is at (-0.04, 0, 5) R_E at 63 s and (0.04, 0, 5) R_E at 64 s. Similarly, the absolute errors in the quadratic gradients $\nabla_2\nabla_2 B_1$ and $\nabla_3\nabla_3 B_1$ were no more than 1 $\mathrm{nT}\cdot\mathrm{R}_E^2$, whereas the relative errors were approximately 30%.

4. Errors

In Section 3, relative error is used to evaluate the truncation error of the proposed method. However, in some cases, evaluation with the relative error is not effective, while the gradient obtained from the accurate model is very small. Furthermore, the truncation error was evaluated under divergence-free magnetic field conditions.

https://doi.org/10.5194/egusphere-2024-1330
Preprint. Discussion started: 17 May 2024

In theory, the divergence of the magnetic field and the gradient of the magnetic field divergence are both exactly zero, as shown by $\nabla \cdot \vec{B} = 0$ and $\left|\nabla\left(\nabla \cdot \vec{B}\right)\right| = 0$. To offer a uniform standard for evaluation, the divergence and gradient of divergence were non-dimensionalized with the corresponding characteristic quantity. The length was calibrated with the spatial characteristic scale of the magnetic structure *D*, and the magnetic field was calibrated with the characteristic magnetic field at the barycentre B_c. Therefore, two evaluation indices were introduced, represented by $\left(\bar{\nabla} \cdot \bar{\vec{B}}\right)_c$ and $\left|\bar{\nabla}\left(\bar{\nabla} \cdot \bar{\vec{B}}\right)_c\right|$. The values of the two indices can be used to evaluate the accuracies of the linear and quadratic gradients derived using the proposed method.

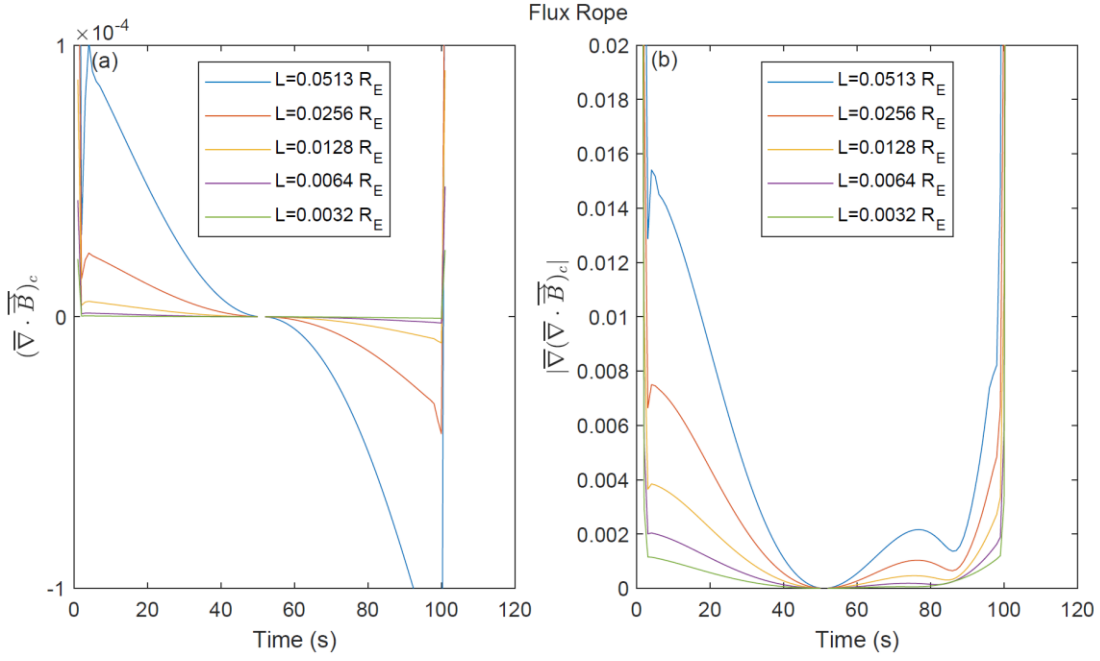

Figure 12. Dimensionless divergence and gradient of divergence for magnetic field along the flux rope crossing path with different characteristic S/C sizes (L).

https://doi.org/10.5194/egusphere-2024-1330
Preprint. Discussion started: 17 May 2024

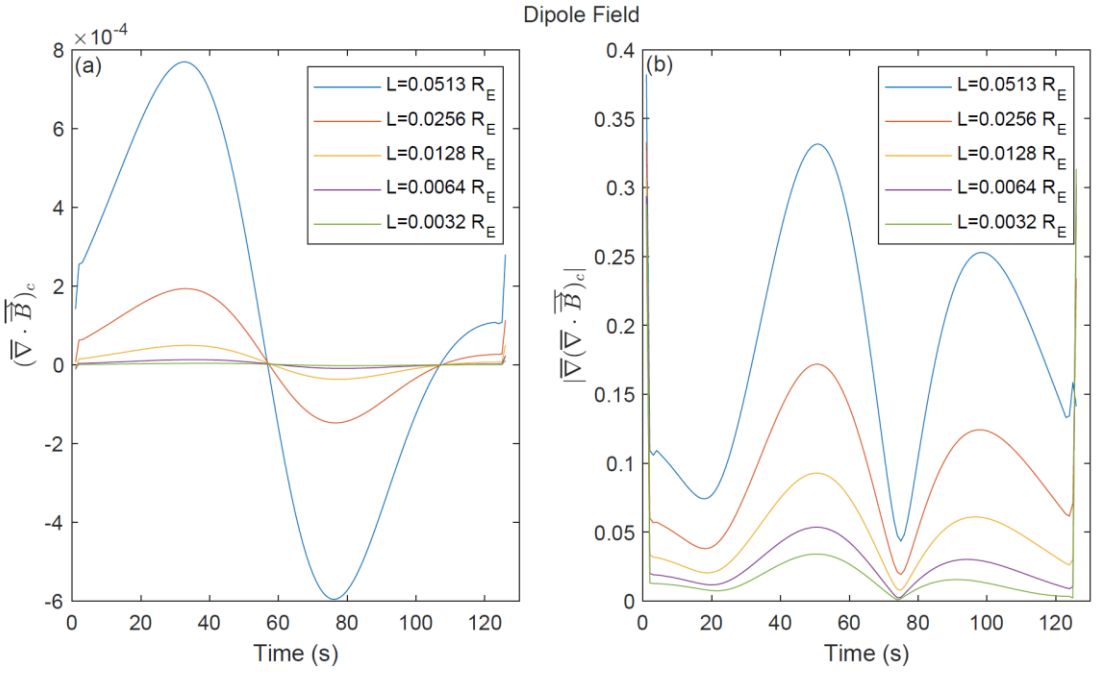

Figure 13. Dimensionless divergence and gradient of divergence for magnetic field along the dipole field crossing path with different characteristic S/C sizes (L).

The algorithm gradients were utilized to calculate the dimensionless divergence and the gradient of divergence for magnetic field at the barycentre along the crossing path with different characteristic S/C sizes, with the results for the flux-rope and dipole-field cases shown in Figure. 12 and 13, respectively. Figure 12 (a) and 13 (a) show that the dimensionless divergence $\left(\bar{\nabla}\cdot\bar{\bar{B}}\right)_c$ at the barycentre is in the order of ten to the minus fourth, while L varies from 0.0032 to 0.0513 R_E. The dimensionless gradient of the divergence $\left|\bar{\nabla}\left(\bar{\nabla}\cdot\bar{\bar{B}}\right)_c\right|$ for the flux-rope case was less than 0.02 with L=0.0513 R_E, as shown in Figure. 12 (b). Similarly, Figure. 13 (b) shows that $\left|\bar{\nabla}\left(\bar{\nabla}\cdot\bar{\bar{B}}\right)_c\right|$ was less than 0.4, with L=0.0513 R_E, for the dipole field. Meanwhile, that $\left|\bar{\nabla}\left(\bar{\nabla}\cdot\bar{\bar{B}}\right)_c\right|$ decreased with decreasing L in both cases. These results confirm the accuracy of the proposed method.

https://doi.org/10.5194/egusphere-2024-1330
Preprint. Discussion started: 17 May 2024

5. Conclusions

In this study, a new algorithm was derived to estimate the linear and quadratic gradients of the magnetic field from 7- or 9-point magnetic measurements to obtain the fine structure of the magnetic field and the magnetic field geometry, allowing elucidation of whether the 7-spacecraft Plasma Observatory and the 9-spacecraft HelioSwarm missions could be utilized for such measurements. By inputting 7–9 point magnetic measurements and using the reference frame transformation relationships of the magnetic field as well as the least-squares method, the new algorithm performs several iterations to finally derive the convergent magnetic linear and quadratic gradients.

The developed algorithm requires fewer restrictions on the spatial configuration of the constellations and only demands that the constellations are non-planar. Actual operating constellations can easily satisfy this constraint. Only magnetic measurements are required, with no other physical measurements needed, and the only physical constraint of the algorithm is the reference-frame transformation relationship of the magnetic field. Divergence-free magnetic field conditions were not required to calculate the magnetic gradient. Alternatively, in the algorithm, the magnitudes of the magnetic divergence and its gradient were used to evaluate the truncation errors of the linear and quadratic magnetic gradients, respectively. The proposed algorithm was verified using a cylindrical force-free flux rope and a dipole magnetic field, with results showing that the iterations effectively converged and that the magnetic gradients can reach reasonable accuracy. The results of this study can thus be applied to the analysis of magnetic field data from multi-spacecraft constellations (e.g., the Plasma Observatory and HelioSwarm) as well as to the design of future constellation missions.

Author contributions

CS designed the method. GZ developed the model code and performed the test. CS and GZ wrote the paper. CS and RK reviewed and edited the paper.

Competing interests

The authors declare that they have no conflict of interest.

Acknowledgments

This work was supported by the National Natural Science Foundation of China (Grant No. 42130202)， National Key Research and Development Program of China (Grant No. 2022YFA1604600) and Hubei Provincial Natural Science Foundation of China (Grant No. 2022CFB928). This research was also supported by the International Space Science Institute

https://doi.org/10.5194/egusphere-2024-1330
Preprint. Discussion started: 17 May 2024

(ISSI) in Bern through the ISSI International Team project #556 (cross-scale energy transfer in space plasmas). We appreciate the reviewer's valuable suggestions.

References

Burch, J. L., Moore, T. E., Torbert, R. B., and Giles, B. L.: Magnetospheric multiscale overview and science objectives, Space Sci. Rev., 199, 5–21. https://doi.org/10.1007/s11214-015-0164-9, 2015.

Burch, J. L. and Phan, T. D.: Magnetic reconnection at the dayside magnetopause: Advances with MMS, Geophys. Res. Lett., 43, 8327–8338. https://doi.org/10.1002/2016GL069787, 2016.

Chanteur, G.: Spatial Interpolation for four spacecraft: Theory, in: Analysis methods for multi-spacecraft data, edited by Paschmann, G. and Daly, P. W., European Space Agency Publ. Division, Noordwijk, Netherlands, 349–370, 1998.

Chanteur, G. and Harvey, C. C.: Spatial interpolation for four spacecraft: Application to magnetic gradients, in: Analysis methods for multi-spacecraft data, edited by Paschmann, G. and Daly, P. W., European Space Agency Publications Division, Noordwijk, Netherlands, 371–394, 1998.

De Keyser, J., Darrouzet, F., Dunlop, M. W., and Décréau, P. M. E.: Least-squares gradient calculation from multi-point observations of scalar and vector fields: Methodology and applications with Cluster in the plasmasphere, Ann. Geophys., 25, 971–987. https://doi.org/10.5194/angeo-25-971-2007, 2007.

De Keyser, J.: Least-squares multi-spacecraft gradient calculation with automatic error estimation, Annales Geophysicae, 26, 3295-3316, https://doi.org/10.5194/angeo-26-3295-2008, 2008.

Dong, X.-C., Dunlop, M. W., Wang, T.-Y., Cao, J.-B., Trattner, K. J., Bamford, R., Russell, C. T., Bingham, R., Strangeway, R. J., Fear, R. C., Giles, B. L., Torbert, R. B.: Carriers and sources of magnetopause current: MMS case study, Journal of Geophysical Research: Space Physics, 123, 5464–5475. https://doi.org/10.1029/2018JA025292, 2018.

Dunlop, M. W., Balogh, A., and Glassmeier, K.-H.: Four-point Cluster application of magnetic field analysis tools: The discontinuity analyzer, J. Geophys. Res., 107, 1385. https://doi.org/10.1029/2001JA005089, 2002a.

Dunlop, M. W., Balogh, A., Glassmeier, K.-H., and Robert, P.: Four-point cluster application of magnetic field analysis tools: The curlometer, J. Geophys. Res., 107, 1384. https://doi.org/10.1029/2001JA005088, 2002b.

Dunlop, M. W., Haaland, S., Escoubet, P. C., and Dong, X.-C.: Commentary on accessing 3-D currents in space: Experiences from Cluster, Journal of Geophysical Research: Space Physics, 121, 7881–7886. https://doi.org/10.1002/2016JA022668, 2016.

Escoubet, C. P., Fehringer, M., and Goldstein, M.: The Cluster mission, Ann. Geophys., 19, 1197–1200. https://doi.org/10.5194/angeo-19-1197-2001, 2001.

Escoubet, C. P., Schmidt, R., and Goldstein, M. L.: Cluster—Science and mission overview, Space Sci. Rev., 79, 11–32. https://doi.org/10.1023/A:1004923124586, 1997.

Haaland, S., Hasegawa, H., Paschmann, G., Sonnerup, B., and Dunlop, M.: 20 years of Cluster observations: The

https://doi.org/10.5194/egusphere-2024-1330
Preprint. Discussion started: 17 May 2024

magnetopause, Journal of Geophysical Research: Space Physics, 126, JA029362, e2021. https://doi.org/10.1029/2021JA029362, 2021.

Hamrin, M., Rönnmark, K., Börlin, N., Vedin, J., and Vaivads, A.: GALS - gradient analysis by least squares, Annales Geophysicae, 26, 3491-3499, https://doi.org/10.5194/angeo-26-3491-2008, 2008.

Harvey, C. C.: Spatial gradients and the volumetric tensor, in: Analysis methods for multi-spacecraft data, edited by Paschmann, G. and Daly, P. W., European Space Agency Publ. Division, Noordwijk, Netherlands, 307–322, 1998.

Liu, Y. Y., Fu, H. S., Olshevsky, V., Pontin, D. I., Liu, C. M., Wang, Z., Chen, G., Dai, L., Retino, A.: SOTE: A nonlinear method for magnetic topology reconstruction in space plasmas, Astrophysical Journal Supplement Series, 244, 31. https://doi.org/10.3847/1538-4365/ab391a, 2019.

Lundquist, S.: Magnetohydrostatic fields, Arkiv för Fysik, 2, 361–365, 1950.

Pitout, F. and Bogdanova, Y. V.: The polar cusp seen by Cluster, Journal of Geophysical Research: Space Physics, 126, JA029582, e2021. https://doi.org/10.1029/2021JA029582, 2021.

Robert, P., Roux, A., Harvey, C. C., Dunlop, M. W., Daly P. W., Glassmeier, K-H.: Tetrahedron geometric factors, in: Analysis methods for multi-spacecraft data, edited by Paschmann, G. and Daly, P. W., European Space Agency Publ. Division, Noordwijk, Netherlands, 323–348, 1998.

Rong, Z. J., Wan, W. X., Shen, C., Li, X., Dunlop, M. W., Petrukovich, A. A., Zhang, T. L., and Lucek, E.: Statistical survey on the magnetic structure in magnetotail current sheets, J. Geophys. Res., 116, A09218. https://doi.org/10.1029/2011JA016489, 2011.

Runov, A., Sergeev, V. A., Nakamura, R., Baumjohann, W., Apatenkov, S., Asano, Y., Takada, T., Volwerk, M., Vörös, Z., Zhang, T. L., Sauvaud, J.-A., Rème, H., Balogh, A.: Local structure of the magnetotail current sheet: 2001 Cluster observations, Ann. Geophys., 24, 247–262. https://doi.org/10.5194/angeo-24-247-2006, 2006.

Russell, C. T., Mellott, M. M., Smith, E. J., and King, J. H.: Multiple spacecraft observations of interplanetary shocks: Four spacecraft determination of shock normals, J. Geophys. Res., 88, 4739–4748. https://doi.org/10.1029/JA088iA06p04739, 1983.

Shen, C., Li, X., Dunlop, M., Liu, Z. X., Balogh, A., Baker, D. N., Hapgood, M., and Wang, X.: Analyses on the geometrical structure of magnetic field in the current sheet based on cluster measurements, J. Geophys. Res., 108, 1168. https://doi.org/10.1029/2002JA009612, 2003.

Shen, C., Liu, Z. X., Li, X., Dunlop, M., Lucek, E., Rong, Z. J., Chen, Z. Q., Escoubet, C. P., Malova, H. V., Lui, A. T. Y., Fazakerley, A., Walsh, A. P., Mouikis, C.: Flattened current sheet and its evolution in substorms, J. Geophys. Res., 113, A07S21. https://doi.org/10.1029/2007JA012812, 2008.

https://doi.org/10.5194/egusphere-2024-1330
Preprint. Discussion started: 17 May 2024

Shen, C., Rong, Z. J., Dunlop, M. W., Ma, Y. H., Li, X., Zeng, G., Yan, G. Q., Wan, W. X., Liu, Z. X., Carr, C. M., Rème, H.: Spatial gradients from irregular, multiple-point spacecraft configurations, J. Geophys. Res., 117, A11207. https://doi.org/10.1029/2012JA018075, 2012.

Shen, C., Yang, Y. Y., Rong, Z. J., Li, X., Dunlop, M., Carr, C. M., Liu, Z. X., Baker, D. N., Chen, Z. Q., Ji, Y., Zeng, G.: Direct calculation of the ring current distribution and magnetic structure seen by Cluster during geomagnetic storms, Journal of Geophysical Research: Space Physics, 119, 2458–2465. https://doi.org/10.1002/2013JA019460, 2014.

Shen, C., Zeng, G., Zhang, C., Rong, Z., Dunlop, M., Russell, C. T., Escoubet, C. P., Ren, N.: Determination of the configurations of boundaries in space, Journal of Geophysical Research: Space Physics, 125, JA028163, e2020. https://doi.org/10.1029/2020JA028163, 2020.

Shen, C., Zhang, C., Rong, Z., Pu, Z., Dunlop, M. W., Escoubet, C. P., Russell, C. T., Zeng, G., Ren, N., Burch, J. L., Zhou, Y.: Nonlinear magnetic gradients and complete magnetic geometry from multispacecraft measurements, Journal of Geophysical Research: Space Physics, 126, JA028846. https://doi.org/10.1029/2020JA028846, 2021a.

Shen, C., Zhou, Y. F., Ma, Y. H., Wang, X. G., Pu, Z. Y., and Dunlop, M.: A general algorithm for the linear and quadratic gradients of physical quantities based on 10 or more point measurements, Journal of Geophysical Research: Space Physics, 126, JA029121, e2021. https://doi.org/10.1029/2021JA029121, 2021b.

Shi, J. K., Cheng, Z. W., Zhang, T. L., Dunlop, M., Liu, Z. X., Torkar, K., Fazakerley, A., Lucek, E., Rème, H., Dandouras, I., Lui, A. T. Y., Pu, Z. Y., Walsh, A. P., Volwerk, M., Lahiff, A. D., Taylor, M. G. G. T., Grocott, A., Kistler, L. M., Lester, M., Mouikis, C., Shen, C.: South-north asymmetry of field-aligned currents in the magnetotail observed by Cluster, J. Geophys. Res., 115, A07228. https://doi.org/10.1029/2009JA014446, 2010.

Shi, Q. Q., Shen, C., Pu, Z. Y., Dunlop, M. W., Zong, Q. G., Zhang, H., Xiao, C. J., Liu, Z. X., and Balogh, A.: Dimensional analysis of observed structures using multipoint magnetic field measurements: Application to Cluster, Geophys. Res. Lett., 32, L12105. https://doi.org/10.1029/2005GL022454, 2005.

Sonnerup, B. U. Ö., Haaland, S., Paschmann, G., Lavraud, B., Dunlop, M. W., Rème, H., and Balogh, A.: Orientation and motion of a discontinuity from single-spacecraft measurements of plasma velocity and density: Minimum mass flux residue, Journal of Geophysical Research: Space Physics, 109, A03221. https://doi.org/10.1029/2003JA010230, 2004.

Torbert, R. B., Dors, I., Argall, M. R., Genestreti, K. J., Burch, J. L., Farrugia, C. J., Forbes, T. G., Giles, B. L., Strangeway, R. J.: A new method of 3-D magnetic field reconstruction, Geophys. Res. Lett., 47, GL085542, e2019. https://doi.org/10.1029/2019GL085542, 2020.

Vogt, J., Albert, A., and Marghitu, O.: Analysis of three-spacecraft data using planar reciprocal vectors: Methodological framework and spatial gradient estimation, Ann. Geophys., 27, 3249–3273. https://doi.org/10.5194/angeo-27-3249-2009, 2009.

Vogt, J., Sorbalo, E., He, M., and Blagau, A.: Gradient estimation using configurations of two or three spacecraft, Ann. Geophys., 31, 1913–1927. https://doi.org/10.5194/angeo-31-1913-2013, 2013.

https://doi.org/10.5194/egusphere-2024-1330
Preprint. Discussion started: 17 May 2024

Zhang, Q. H., Dunlop, M. W., Lockwood, M., Holme, R., Kamide, Y., Baumjohann, W., Liu, R. Y., Yang, H. G., Woodfield, E. E., Hu, H. Q., Zhang, B. C., Liu, S. L.: The distribution of the ring current: Cluster observations, Ann. Geophys., 29, 1655–1662. https://doi.org/10.5194/angeo-29-1655-2011, 2011.

Zhou, Y. and Shen, C.: Estimating gradients of physical fields in space, Ann. Geophys., 42, 17–28. https://doi.org/10.5194/angeo-42-17-2024, 2024.